Electron-Beam-Induced Substitutional Carbon Doping of Boron Nitride Nanosheets, Nanoribbons, and Nanotubes

Xianlong Wei,* Ming-Sheng Wang, Yoshio Bando, and Dmitri Golberg*

International Center for Materials Nanoarchitectonics (MANA), National Institute for Materials Science (NIMS), Namiki 1-1, Tsukuba, Ibaraki, 305-0044, Japan

ABSTRACT Substitutional carbon doping of the honeycomb-like boron nitride (BN) lattices in two-dimensional (nanosheets) and one-dimensional (nanoribbons and nanotubes) nanostructures was achieved *via in situ* electron beam irradiation in an energy-filtering 300 kV high-resolution transmission electron microscope using a C atoms feedstock intentionally introduced into the microscope. The C substitutions for B and N atoms in the honeycomb lattices were demonstrated through electron energy loss spectroscopy, spatially resolved energy-filtered elemental mapping, and *in situ* electrical measurements. The preferential doping was found to occur at the sites more vulnerable to electron beam irradiation. This transformed BN nanostructures from electrical insulators to conductors. It was shown that B and N atoms in a BN nanotube could be nearly completely replaced with C atoms *via* electron-beam-induced doping. The doping mechanism was proposed to rely on the knockout ejections of B and N atoms and subsequent healing of vacancies with supplying C atoms.

KEYWORDS: electron-beam-induced doping · boron nitride nanosheet · boron nitride nanoribbon · boron nitride nanotube

Honeycomb-network-based carbon nanostructures (e.g., carbon nanotubes (CNTs), graphenes, and graphene nanoribbons) have been in the forefront of materials science over the past two decades due to their unique and fascinating properties and promising potential applications. As an analogue of the carbon honeycomb lattice in which C atoms are fully substituted with alternating B and N atoms, a monatomic boron nitride (BN) honeycomb lattice has been demonstrated to exhibit the same versatility as its C counterpart and to form diverse two-dimensional and one-dimensional morphologies, *e.g.*, BN nanosheets (BNNSs), nanoribbons (BNNRs), and nanotubes (BNNTs).[1−3] Even though these BN nanostructures have lattice parameters very close to their C counterparts, different elemental components give them quite different physical properties. BN nanostructure aggregates display a "snow-white" color appearance, while those of C are pitch-black.[1] Also BNNTs exhibit much better chemical and thermal stabilities compared to CNTs and, at the same time, possess a similarly high thermal conductivity and excellent mechanical properties.[1,4] Such outstanding performances are also expected to be peculiar to BNNSs and BNNRs.[2] However, the most significant differences in physical properties of C and BN nanostructures are their electrical performances. For example, BNNTs and BNNSs are electrically insulating with a bandgap of ∼5−6 eV independent of their morphologies and structures,[2] while CNTs are metallic or narrow-bandgap semiconducting depending on their chirality, and graphenes are semimetallic with zero bandgap.[5] Nearly identical honeycomb structures of BN and C systems with almost the same lattice parameters make it possible to construct hybrid ternary B−C−N honeycomb lattices and corresponding B−C−N nanostructures with electrical properties intermediate between those of pure BN and C systems.[6−8] B−C−N nanotubes have previously been obtained by doping CNTs with B and N or inverse doping of BNNTs with C, and, in fact, such structures exhibited tunable semiconductivity.[6,9,10] Recently, atomic layers with hybridized BN and C domains have also been successfully synthesized, and their conductivity has been demonstrated to increase with C content.[11] Furthermore, B−C−N nanosheets and nanoribbons were predicted to exhibit interesting electrical and magnetic properties depending on elemental contents and the atomic species arrangements within the honeycomb networks.[12−15] Therefore, this approach offers a rare possibility of delicate tailoring of electrical and magnetic properties of B−C−N

* Address correspondence to WEI.Xianlong@nims.go.jp (or weixl@pku.edu.cn), GOLBERG.Dmitri@nims.go.jp.

Received for review December 21, 2010 and accepted March 22, 2011.

Published online March 22, 2011
10.1021/nn103548r

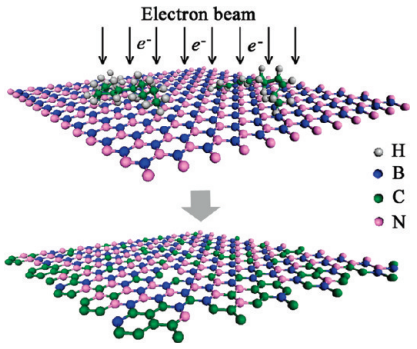

Figure 1. Schematic drawing of electron-beam-induced substitutional C doping in a honeycomb BN lattice. Some defects are also introduced into the lattice, especially at its edges, during doping. C doping preferentially takes place at the damaged edges.

nanostructures by constructing well-defined B−C−N honeycomb lattices. Even though such B−C−N structures in the form of nanotubes and nanosheets have previously been obtained by chemical syntheses or doping,[6,8,11] a general method for constructing them in the form of nanosheets, nanoribbons, and nanotubes has never been developed.

Recently, we have found that C substitution for B and N atoms in BNNTs can be achieved *via in situ* electron beam irradiation inside a transmission electron microscope (TEM).[10] Herein, we show that such electron-beam-induced substitutional C doping can also take place in the honeycomb lattices of BNNSs and BNNRs. This work provides a general method for constructing B−C−N honeycomb structures in the form of nanosheets, nanoribbons, and nanotubes. We also show that B and N atoms in a BN network can nearly completely be substituted by C atoms under electron-beam-induced doping. Therefore, such doping provides a promising route toward on-demand tailoring of electrical properties of diverse BN nanostructures in a full composition range between pure BN and C systems.

RESULTS AND DISCUSSION

The experiments were *in situ* performed at room temperature inside an energy-filtering 300 kV JEOL 3100FEF (Omega Filter) high-resolution TEM equipped with a scanning tunneling microscope (STM)-TEM Nanofactory Instruments holder. "Snow-white", entirely pure BN nanostructures synthesized by an induction heating method were used in our experiments.[16,17] The as-synthesized product mainly consists of BNNTs. However, a small amount of byproduct nanosheets and unfolded nanotubes or nanoribbons could also occasionally be found in it (see Figure S1a in the Supporting Information). The core-loss K-edges of B at 188 eV and N at 401 eV with well-defined sharp π^* and σ^* peaks in the electron energy loss (EEL) spectrum indicate that the BN nanostructures are highly pure, well-structured, and sp^2-hybridized (see Figure S1b in the Supporting Information).

A carbon source was deliberately introduced into the column of the TEM by placing a tiny amount of paraffin wax (C_nH_{2n+2} with $19 \leq n \leq 36$) several millimeters away of BN nanostructures. It provided the needed C feedstock for C substitutions for B and N atoms in a BN honeycomb lattice. The introduction of paraffin wax results in the diffusion and adsorption of hydrocarbon molecules on the surfaces, including the surfaces of BN nanostructures, located near the paraffin droplets.[18] When irradiated with electrons, the absorbed hydrocarbon molecules are decomposed, giving birth to free C species.[18] We will show that under irradiation with a high-energy electron beam, the C atoms decomposed from hydrocarbon molecules can be substituted for B and N atoms in the honeycomb lattices of BNNSs and BNNRs in the same way as they are in BNNTs, as we previously stated.[10] Figure 1 shows a schematic drawing of C substitution for B and N in a BN lattice under electron beam irradiation. In order to confirm C substitution for B and N atoms, we studied the elemental components, their spatial distributions, and electrical properties of the doped nanostructures by means of electron energy loss spectroscopy, spatially resolved energy-filtered elemental mapping, and in-tandem *in situ* electrical measurements.

Figure 2 shows the results obtained from a BNNS that was placed between the Au wire edge and a W probe (Figure 2a). Selected area electron diffraction pattern of the BNNS clearly revealed a hexagonal honeycomb structure (inset of Figure 2a). Figure 2b is the EEL spectra taken from the BNNS before and after it was irradiated by an electron beam in the presence of paraffin wax. In addition to the core-loss K-edges of B and N, the core-loss K-edge of C at 284 eV with well-defined sharp π^* and σ^* peaks was also identified in the EEL spectrum taken after such electron beam irradiation, which clearly indicated that sp^2-hybridized C atoms had been incorporated into the BNNS. Quantification of the EEL spectrum gave a B/C/N atomic ratio of $1.00{:}0.43 \pm 0.06{:}0.96 \pm 0.14$ and a C content of 17.8 at. %. To further explore the detailed elemental distributions, energy-filtered B, C, and N maps of the BNNS were constructed (Figure 2c−e). It can be seen from the C map that there was a significant amount of C incorporation within the BNNS. However, in contrast to uniform distributions of B and N, there was C enrichment at the BNNS edges and within some internal areas. This indicates that the C incorporation preferentially takes place at these particular sites.

A high-resolution TEM image (Figure 2g) showed that the BNNS was a multilayer nanosheet with an edge width of ~7 nm (corresponding to ~20 monatomic BN layers) and that the outermost edges of the BNNS were seriously damaged by the electron beam irradiation. These exhibited wavy and disordered morphologies, whereas the inner edges were still

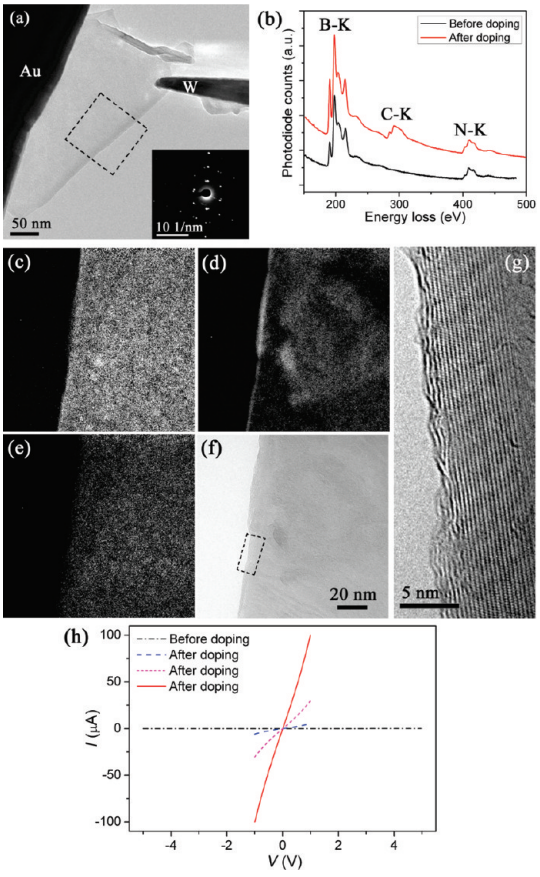

Figure 2. (a) TEM image showing a BNNS placed between an Au electrode and a W probe. The inset is a selected area electron diffraction pattern of the BNNS. (b) EEL spectra of the BNNS before and after doping. (c–f) Energy-filtered elemental maps (B (c), C (d), and N (e)) and corresponding zero-loss image (f) of the doped BNNS. (g) HRTEM image of the framed area in (f). (h) Two-terminal *I*–*V* curves of the BNNS before and after doping. The curves after doping correspond to different doping times. The longer the BNNS was doped, the higher conductance it showed.

well-structured and displayed well-defined lattice fringes. The much more severe damage of the outermost edges was also observed in pure BN nanosheets (see Figure S2 in the Supporting Information) and is thought to be caused by two reasons. First, compared to three-coordinated atoms in the interior of a nanosheet, two- or one-coordinated B/N atoms at the edges have lower threshold energies for knockout ejection and are more easily sputtered off (Figure 1).[19] Second, for a multilayer BN nanosheet, the B/N atoms were found to be mainly sputtered from the electron beam exit surface layers,[20] which correspond to the outermost edges of the nanosheet. A careful comparison between the C map (Figure 2d) and high-resolution TEM image (Figure 2g) indicates that C incorporation preferentially takes place at the damaged edges.

Carbon species could be added to a BN material in two ways: as a separated C phase coating on the pristine BNNS as a result of electron-beam-induced C deposition or as C substitution for B and N atoms within the honeycomb lattices under crystallization of a hybrid B–C–N phase. The following two reasons make us conclude that C is incorporated in the latter way and in the same fashion as in the case of BNNTs analyzed by us previously.[10] First, there were no separate C phase coating layers seen (usually this is an amorphous-like phase formed under C deposition induced by electron beam irradiation[21]) on the BNNS edge, as revealed by high-resolution TEM (HRTEM) imaging. Second, no local preference for C incorporation at the edges would be expected if such a process resulted from the electron-beam-induced C deposition. The preferential C doping at the damaged BN film edges indicates that the doping is closely related to electron-beam-induced damage, which agrees well with the previously proposed by us substitutional doping mechanism based on knockout ejections of B and N atoms.[10] The presence of preferential C doping sites implies that C phase domains in doped BN nanostructures tend to be segregated.[22,23]

The substitutional C doping was further confirmed by *in situ* two-terminal electrical measurements on the same BNNS before and after doping (Figure 2h). The BNNS was electrically insulating with no measurable current under a bias voltage up to 10 V before doping, which is in agreement with a 5.5 eV wide bandgap of BNNSs and previous measurements.[11,24] However, when the BNNS was irradiated under electron beam for doping, its electrical conductivity increased gradually and continuously with irradiation time, and a linear *I*–*V* curve with a resistance as low as ~10 KΩ was finally recorded. This indicates that substitutional C doping has transformed the BNNS from an electrical insulator to a conductor. A conductivity increase with irradiation time was attributed to the increase of C content. The metallic character of the doped BNNS agrees well with the previous theoretical predictions and experiments on B–C–N hybrid nanosheets.[11,12]

Similar results were also obtained on BNNRs. Figure 3a displays a curved BNNR with an increasing curvature along its axis (schematically shown in the inset of Figure 3a) and connected between an Au wire edge and a W probe. EEL spectra of the BNNR before and after its irradiation with an electron beam (again under the presence of a paraffin wax droplet in the BNNR vicinity) are shown in Figure 3b. As compared to the EEL spectrum before doping, the core-loss K-edges of B, C, and N with sharp π^* and σ^* peaks can all be clearly identified in the EEL spectrum after doping, which indicates that sp^2-hybridized C atoms have been introduced into the ribbon. The quantification of the EEL spectrum gave a B/C/N atomic ratio of 1.00:0.15 ± 0.02:0.93 ± 0.13 and a C content of 7.0 at. %. Spatially resolved energy-filtered elemental maps demonstrating detailed elemental distributions are shown in Figure 3c–e. It can be seen that the intensity profiles

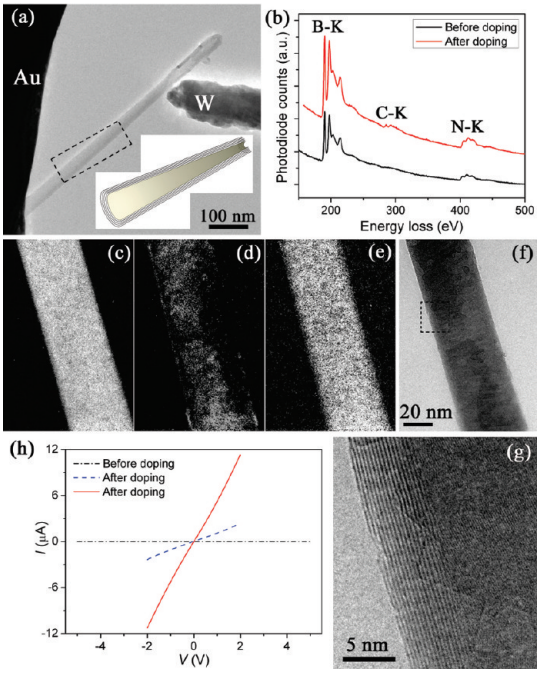

Figure 3. (a) TEM image showing a curved BNNR with an increasing curvature along its axis. BNNR is placed between an Au electrode and a W probe. The inset is a schematic drawing of the BNNR. (b) EEL spectra of the nanoribbon before and after doping. (c–f) Energy-filtered elemental maps (B (c), C (d), and N (e)) and corresponding zero-loss image (f) of the doped nanoribbon. (g) High-resolution TEM image of the framed area in (f). (h) Two-terminal *I*–*V* curves of the nanoribbon before and after doping. The curves after doping correspond to different doping times. The longer the BNNS was doped, the higher conductance it showed.

in B, C, and N maps are of nearly the same width. Similar to the case of BNNS, there is a higher C content at the edges and within some flaked internal areas as compared to uniform distributions of B and N species. The HRTEM image (Figure 3g) shows that there is no separate C deposition layer, but what is apparent is the electron-beam-induced defects at the ribbon edges. This indicates that C atoms have been incorporated into BNNR in the same manner as in the case of BNNS, *i.e.*, *via* C substitution for B and N atoms in the honeycomb network. The rough surface of the outermost areas, as shown in Figure 3f, is a common feature of as-synthesized BNNRs (see Figure S3 in the Supporting Information). The higher C content at these areas agrees well with the preferential doping at damaged edges, since such domains are more vulnerable than perfect BN surfaces due to an increased number of defects.

Two-terminal electrical measurements were also performed on the same BNNR before and after C doping (Figure 3h). Before doping, the BNNR was an insulator with no measurable current under 10 V voltage, in agreement with the previous theoretical predictions of a wide bandgap in BNNRs (~3.8 eV for zigzag nanoribbons and ~4.5 eV for armchair nanoribbons).[25] After doping, a linear *I*–*V* curve with a resistance as low as ~200 KΩ was finally recorded. Here, for the first time we experimentally show that, similarly to the other two morphologies, *i.e.*, BNNSs and BNNTs, BNNRs can also be transformed from insulators to conductors through intentional C doping. The metallic character of the B–C–N nanoribbon agrees well with the previous theoretical calculations.[13–15] Recently, BNNRs with substitutional C edges were predicted to have widely tunable electrical and magnetic properties exhibiting half-semiconducting → half-metallic → metallic behavior transitions depending on doping concentrations.[15] The preferential C substitutions at the BNNR edges, as shown in Figure 3d, in fact make it possible to widely tune electrical and magnetic properties of BNNRs *via* designed electron-beam-induced C doping.

The mechanism of substitutional C doping of the BNNS and BNNR is thought to be the same as that earlier uncovered by us for BNNTs,[10] *i.e.*, knockout ejections of B and N atoms from honeycomb BN lattices and subsequent healing of the created vacancies with C atoms.[10] Threshold electron beam energies for B and N atom ejections from a monolayer BNNS were computed to be 74 and 84 keV (in the earlier work)[22] or 79.5 and 118.6 keV (in the latest report).[19] B and N atom ejections from BNNSs were experimentally observed under bombardment with an electron beam of 80 and 120 keV.[20,26] So, a working voltage of 300 kV in our experiments is high enough to knock out B and N atoms from the BN lattice of a nanosheet or a nanoribbon. Since the formation energies of substitutional C defects at both B and N sites were predicted to be lower than those of B and N vacancies in a BN monolayer, the B and N vacancies produced by knockout ejection would immediately be filled by supplying C atoms originated from decomposed hydrocarbon molecules.[27] Actually, the knockout ejections of B and N atoms from a monolayer BNNS and subsequent healing of the vacancies with C atoms have recently been directly traced by annular dark-field electron microscopy.[28] The proposed doping mechanism can explain why C doping preferentially takes place at the sites more vulnerable to the electron beam irradiation, such as the edges of BN nanosheets and nanoribbons, and at the sites of wrinkled outermost portions.

In addition to elemental distributions, the B/C/N atomic ratio of B–C–N hybrid nanostructures is another key factor determining the resultant physical properties. Therefore, how high the C concentration in a honeycomb lattice can be achieved *via* the above-described electron-beam-induced doping is an important question to be answered. On the basis of a careful analysis of elemental distributions of a doped BNNT and a careful comparison of the tube structures before and after doping, we found that a few outer shells of a BNNT could nearly completely be transformed to pure C shells *via* the developed doping process.

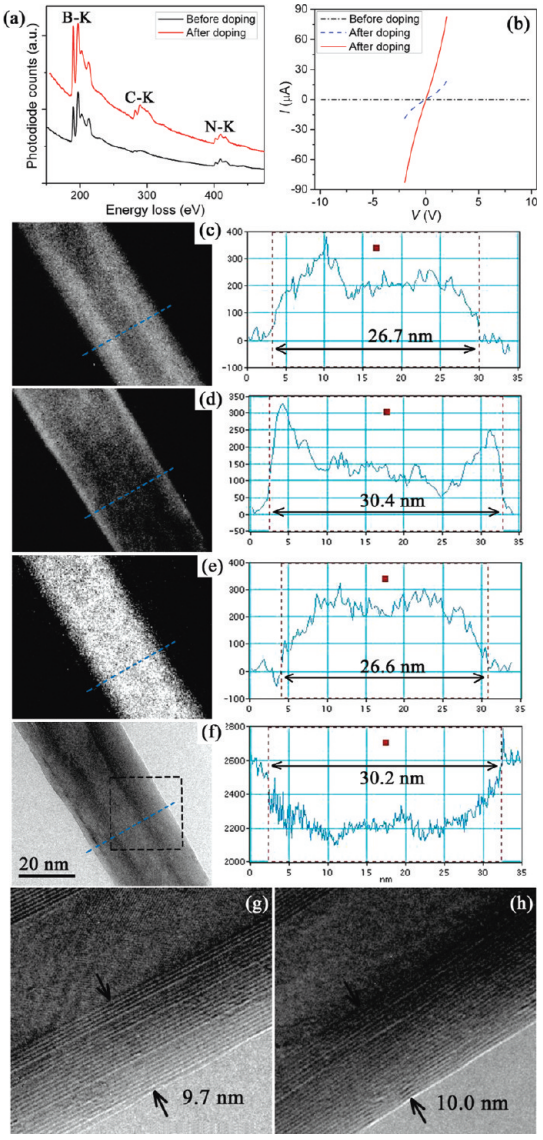

Figure 4. (a) EEL spectra of a BNNT before and after doping. (b) Two-terminal *I*−*V* curves of the tube before and after doping. The curves after doping correspond to different doping times (dashed line, shorter time; solid line, longer time). (c−f) Energy-filtered elemental maps (B (c), C (d), and N (e)) and zero-loss image (f) of the tube, and the corresponding intensity profiles along the dashed line in each figure. (g, h) HRTEM images of the framed area in (f) before (g) and after (h) C doping.

Figure 4a shows EEL spectra of a multiwalled BN nanotube before and after doping. The quantification of the EEL spectrum after doping gave a B/C/N atomic ratio of 1.00:0.66 ± 0.09:0.89 ± 0.13 and an overall C content of ~25.9 at. %. The C incorporation transformed the tube from an electrical insulator to a conductor (Figure 4b). Figure 4c−e shows detailed spatial distributions of B, C, and N in the doped tube. The width of the intensity profile in the C map is measured to be 30.4 nm, which is in good agreement with the tube diameter of 30.2 nm measured on the zero-loss image (Figure 4f), but ~3.7 nm larger than those in B (26.7 nm) and N (26.6 nm) maps. The difference in profile widths as large as ~3.7 nm cannot be attributed to the measurement errors considering a spatial resolution of 0.5 nm during mapping. This undoubtedly indicates that a few outer layers of the doped tube have eventually become nearly pure C since a minimum detectable mass fraction of energy-filtered elemental mapping of less than ~5 at. % is expected.

To explore the origin of the present phenomenon, we made a careful comparison of the tube structures before (Figure 4g) and after (Figure 4h) doping. There were totally 26 tubular layers with a thickness of 9.7 nm before doping, while after doping there were totally 27 layers with a thickness of 10.0 nm. The added layer may be an internal BN layer, whose image can appear or disappear depending on tube orientation around its circumference relative to TEM electron beam incidence and due to the presence of dislocations, or a newly coated C layer on the surface of the pristine BNNT formed due to the electron-beam-induced C deposition and/or Joule-heating annealing. The C-coated layers maybe formed if the decomposition rate of C atoms is faster than the substitution rate of C atoms for B/N atoms. However, even though it was the latter case, the coating of only one C layer could not fully account for the outer, nearly pure C layer shield as thick as ~1.8 nm, as obtained from elemental maps, and also a C concentration of as high as ~25.9 at. %, which corresponds to about six pure C layers (if the coating of pure C layers on pure BN layers is assumed). Therefore, the outer C layers in the doped tube resulted from a nearly complete C substitution for B and N atoms within the pristine BN tubular layers. In other words, starting honeycomb BN lattices of the outer shells of the BNNT were nearly completely replaced by C shells *via* electron beam irradiation. Since the electrical properties of hybrid B−C−N nanostructures are supposed to be intermediate between those peculiar to pure BN and C systems (depending on atomic ratios and distributions),[9] an opportunity of nearly complete C substitution for B and N atoms in the honeycomb BN lattices makes it possible to controllably tune the electrical properties of B−C−N nanostructures in a full range of compositions, between pure BN and C, *via* the designed doping technique.

A comparison of C substitution was made among the three different BN nanostructures. Compared to C distributions in the doped nanosheet (Figure 2d) and nanoribbon (Figure 3d), where C substitution preferentially takes place at the sites more vulnerable to electron beam irradiation (edges, flaked areas, *etc.*), C distribution of the BNNT seems to be more homogeneous and uniform. This is thought to result from the lack of preferable doping sites since a BNNT is formed from perfectly rolled honeycomb lattices without exposed edges. The C substitution in different kinds of BN nanostructures showed no obvious dependence on

their width or curvature. This is understandable when considering the mechanism of C doping. The C substitution was proposed to rely on the knockout ejections of B and C atoms and subsequent healing of vacancies with C atoms. These two processes have no dependence on the width of nanostructures if they are wide enough (width range of >40 nm that we studied). Even though they are thought to depend on the strain energy of chemical bonds, and thus curvature of BN nanostructures, the effect is too small to be detected for BN nanotubes we studied due to their relatively large diameters of ~30 nm, considering the fact that the strain energy per atom is inversely proportional to the square of the tube diameter.[5]

To sum up, substitutional C doping of the honeycomb lattices in BN nanosheets, nanoribbons, and nanotubes was achieved *via in situ* electron beam irradiation inside the TEM using a deliberately introduced C feedstock. The compositions, elemental distributions, and electrical properties of C-doped BN nanostructures were thoroughly studied using EEL spectroscopy, energy-filtered elemental mappings, and *in situ* electrical measurements. C substitutions for B and N atoms were found to preferentially occur at the sites more vulnerable to electron beam irradiation, such as BNNS and BNNR edges, and the wrinkled domains on the outermost surface. This agrees well with the proposed doping mechanism that presumes knockout ejections of B and N atoms from honeycomb BN lattices and subsequent healing of the vacancies with supplied C atoms. Careful analysis of elemental distributions within a doped BNNT and its structures before and after doping indicated that BN honeycomb lattices could nearly completely be substituted by C atoms *via* electron-beam-induced doping. C substitutions transformed these BN nanostructures from electrical insulators to conductors. The designed doping procedure is envisaged to become a promising method for on-demand tuning of electrical and magnetic properties of B–C–N nanostructures in a full range of ternary B–C–N compositions.

METHODS

"Snow-white" purity BN nanostructures synthesized *via* an induction heating method were transferred into the TEM (JEOL 3100FEF) using an Au wire with a flattened and sharpened edge. The Au wire was dipped into the aggregation of as-synthesized powder-like products, which would cause some nanostructures to adhere to its edge (Figure S1a). The Au wire was then mounted on the fixed terminal of the STM-TEM Nanofactory Instruments holder. A chemically etched W tip was mounted on the movable terminal of the STM-TEM holder, which could move in three dimensions under a piezoelectric tube drive with a precision of ~1 nm. The Au wire and W tip can act as two electrical probes to perform two-terminal electrical measurements on a BN nanostructure placed between them. Under TEM observations, a particular BN nanostructure was first selected. Then its compositions and electrical properties were determined through EEL spectroscopy and *in situ* electrical measurements. In order to dope the BN nanostructure with C, a tiny amount of paraffin wax was attached to the W tip, about several millimeters away from the tip end, and the BN nanostructure was irradiated with an electron beam. In order to avoid serious structural damages under intense electron irradiation, we usually did not focus an electron beam directly onto the BN nanostructure of interest, but focused it on the Au wire edge near it, which caused the BN nanostructure to be irradiated under the backscattered and secondary electrons. This kind of secondary electron beam irradiation was found to be more efficient for C doping than direct electron beam irradiation. After doping, atomic structure, composition, elemental distributions, and electrical properties of the object of interest were measured once again. In order to avoid serious structural damages under intense electron beam irradiation while taking EEL spectra and acquiring energy-filtered elemental maps, an electrical current of tens of μA was applied to the doped BN nanostructures once they became conducting. The Joule heating could prevent further structural damage and even induce annealing of doped nanostructures. Without such Joule heating, BN lattices can be severely destroyed by an electron beam and become amorphous (see Figure S2 in the Supporting Information). Energy-filtered elemental maps were acquired through a three-window procedure based on two pre-edge and one post-edge energy-filtered images. The energy filter slit width was set at 10 eV for B maps and zero-loss images and 20 eV for C and N maps.

Acknowledgment. This work was supported by the International Center for Materials Nanoarchitectonics (MANA) of the National Institute for Materials Science (NIMS).

Supporting Information Available: Structures and compositions of as-synthesized BN nanostructures, structure evolution of a BN nanosheet under 300 kV electron beam irradiation, and the rough surface of as-synthesized BN nanoribbons. This material is available free of charge *via* the Internet at http://pubs.acs.org.

REFERENCES AND NOTES

1. Golberg, D.; Bando, Y.; Tang, C. C.; Zhi, C. Y. Boron Nitride Nanotubes. *Adv. Mater.* **2007,** *19*, 2413–2432.
2. Golberg, D.; Bando, Y.; Huang, Y.; Terao, T.; Mitome, M.; Tang, C.; Zhi, C. Y. Boron Nitride Nanotubes and Nanosheets. *ACS Nano* **2010,** *4*, 2979–2993.
3. Zeng, H.; Zhi, C. Y.; Zhang, Z.; Wei, X.; Wang, X.; Guo, W.; Bando, Y.; Golberg, D. "White Graphenes": Boron Nitride Nanoribbons *via* Boron Nitride Nanotube Unwrapping. *Nano Lett.* **2010,** *10*, 5049–5055.
4. Wei, X. L.; Wang, M.-S.; Bando, Y.; Golberg, D. Tensile Tests on Individual Multi-Walled Boron Nitride Nanotubes. *Adv. Mater.* **2010,** *22*, 4895–4899.
5. Saito, R., Dresselhaus, G.; Dresselhaus, M. S. *Physical Properties of Carbon Nanotubes*; Imperial College Press: London, 2003.
6. Stephan, O.; Ajayan, P. M.; Colliex, C.; Redlich, P.; Lambert, J. M.; Bernier, P.; Lefin, P. Doping Graphitic and Carbon Nanotube Structures with Boron and Nitrogen. *Science* **1994,** *266*, 1683–1685.
7. Zhang, Y.; Gu, H.; Suenaga, K.; Iijima, S. Heterogeneous Growth of B-C-N Nanotubes by Laser Ablation. *Chem. Phys. Lett.* **1997,** *279*, 264–269.
8. Weng-Sieh, Z.; Cherrey, K.; Chopra, N. G.; Blase, X.; Miyamoto, Y.; Rubio, A.; Cohen, M. L.; Louie, S. G.; Zettl, A.; Gronsky, R. Synthesis of $B_xC_yN_z$ Nanotubules. *Phys. Rev. B* **1995,** *51*, 11229–11232.
9. Golberg, D.; Bando, Y.; Dorozhkin, P.; Dong, Z. C. Synthesis, Analysis, and Electrical Property Measurements of

Compound Nanotubes in the B-C-N Ceramic System. *MRS Bull.* **2004,** *29*, 38–42.
10. Wei, X. L.; Wang, M. S.; Bando, Y.; Golberg, D. Post-Synthesis Carbon Doping of Individual Multiwalled Boron Nitride Nanotubes via Electron-Beam Irradiation. *J. Am. Chem. Soc.* **2010,** *132*, 13592–13593.
11. Ci, L.; Song, L.; Jin, C.; Jariwala, D.; Wu, D.; Li, Y.; Srivastava, A.; Wang, Z. F.; Storr, K.; Balicas, L. M.; *et al*. Atomic Layers of Hybridized Boron Nitride and Graphene Domains. *Nat. Mater.* **2010,** *9*, 430–435.
12. Mazzoni, M.; Nunes, R.; Azevedo, S.; Chacham, H. Electronic Structure and Energetics of BxCyNz Layered Structures. *Phys. Rev. B* **2006,** *73*, 073108.
13. Nakamura, J.; Nitta, T.; Natori, A. Electronic and Magnetic Properties of BNC Ribbons. *Phys. Rev. B* **2005,** *72*, 205429.
14. Kan, E.-J.; Wu, X.; Li, Z.; Zeng, X. C.; Yang, J.; Hou, J. G. Half-metallicity in Hybrid BCN Nanoribbons. *J. Chem. Phys.* **2008,** *129*, 084712.
15. Tang, S.; Cao, Z. Carbon-doped Zigzag Boron Nitride Nanoribbons with Widely Tunable Electronic and Magnetic Properties: Insight from Density Functional Calculations. *Phys. Chem. Chem. Phys.* **2010,** *12*, 2313.
16. Tang, C.; Bando, Y.; Sato, T.; Kurashima, K. A Novel Precursor for Synthesis of Pure Boron Nitride Nanotubes. *Chem. Commun.* **2002,** *12*, 1290–1291.
17. Zhi, C. Y.; Bando, Y.; Tan, C. C.; Golberg, D. Effective Precursor for High Yield Synthesis of Pure BN Nanotubes. *Solid State Commun.* **2005,** *135*, 67–70.
18. Ding, W.; Dikin, D. A.; Chen, X.; Piner, R. D.; Ruoff, R. S.; Zussman, E.; Wang, X.; Li, X. Mechanics of Hydrogenated Amorphous Carbon Deposits from Electron-Beam-Induced Deposition of a Paraffin Precursor. *J. Appl. Phys.* **2005,** *98*, 014905.
19. Kotakoski, J.; Jin, C. H.; Lehtinen, O.; Suenaga, K.; Krasheninnikov, A. V. Electron Knock-on Damage in Hexagonal Boron Nitride Monolayers. *Phys. Rev. B* **2010,** *82*, 113404.
20. Meyer, J. C.; Chuvilin, A.; Algara-Siller, G.; Biskupek, J.; Kaiser, U. Selective Sputtering and Atomic Resolution Imaging of Atomically Thin Boron Nitride Membranes. *Nano Lett.* **2009,** *9*, 2683–2689.
21. Wang, M. S.; Wang, J. Y.; Chen, Q.; Peng, L. M. Fabrication and Electrical and Mechanical Properties of Carbon Nanotube Interconnections. *Adv. Funct. Mater.* **2005,** *15*, 1825–1831.
22. Kohler-Redlich, P.; Terrones, M.; Manteca-Diego, C.; Hsu, W. K.; Terrones, H.; Ruhle, M.; Kroto, H. W.; Walton, D. R. M. Stable BC_2N Nanostructures: Low-temperature Production of Segregated C/BN Layered Materials. *Chem. Phys. Lett.* **1999,** *310*, 459–465.
23. Enouz, S.; Stéphan, O.; Cochon, J.-L.; Colliex, C.; Loiseau, A. C-BN Patterned Single-Walled Nanotubes Synthesized by Laser Vaporization. *Nano Lett.* **2007,** *7*, 1856–1862.
24. Song, L.; Ci, L.; Lu, H.; Sorokin, P. B.; Jin, C.; Ni, J.; Kvashnin, A. G.; Kvashnin, D. G.; Lou, J.; Yakobson, B. I.; *et al*. Large Scale Growth and Characterization of Atomic Hexagonal Boron Nitride Layers. *Nano Lett.* **2010,** *10*, 3209–3215.
25. Park, C. H.; Louie, S. G. Energy Gaps and Stark Effect in Boron Nitride Nanoribbons. *Nano Lett.* **2008,** *8*, 2200–2203.
26. Jin, C. H.; Lin, F.; Suenaga, K.; Iijima, S. Fabrication of a Freestanding Boron Nitride Single Layer and Its Defect Assignments. *Phys. Rev. Lett.* **2009,** *102*, 195505.
27. Azevedo, S.; Kaschny, J. R.; de Castilho, C. M. C.; Mota, F. D. A Theoretical Investigation of Defects in a Boron Nitride Monolayer. *Nanotechnology* **2007,** *18*, 495707.
28. Krivanek, O. L.; Chisholm, M. F.; Nicolosi, V.; Pennycook, T. J.; Corbin, G. J.; Dellby, N.; Murfitt, M. F.; Own, C. S.; Szilagyi, Z. S.; Oxley, M. P.; *et al*. Atom-by-Atom Structural and Chemical Analysis by Annular Dark-Field Electron Microscopy. *Nature* **2010,** *464*, 571–574.